Raman Lidar Installed at Southern Great Plains Cloud and Radiation Testbed Site for Profiling Atmospheric Water Vapor, Aerosols, and Clouds

J.E.M. Goldsmith, S. E. Bisson, and F. H. Blair
Sandia National Laboratories
Livermore, California

We have developed a ruggedized Raman lidar system that resides permanently at the Southern Great Plains (SGP) Cloud and Radiation Testbed (CART) site, providing vertical profiles of water vapor, aerosols, and clouds. The CART Raman Lidar was delivered to the site on September 13, 1995, and became operational on September 19, in time to support the ARM Enhanced Shortwave Experiment (ARESE) campaign.

Raman lidar systems detect selected species by monitoring the wavelength-shifted molecular return produced by Raman scattering from the chosen molecule or molecules. For water-vapor measurements (the key measurement provided by the CART Raman lidar), a nitrogen Raman signal is observed simultaneously with the water-vapor Raman signal; proper ratioing of the signals yields the water-vapor mixing ratio. Similarly, by simultaneously recording the backscatter signal at the laser wavelength (which contains contributions from both Rayleigh and aerosol scattering), the ratio of the backscatter signal to the nitrogen Raman signal yields a quantitative measurement of the aerosol scattering ratio. A variety of aerosol and cloud parameters can be derived from this measurement. In aerosol-free regions of the atmosphere, temperature profiles can be derived from the density measurements obtained from the nitrogen Raman signal. Finally, polarizing optics and an additional direct-backscatter channel provide depolarization measurements, yielding additional information on particle shape, of special interest for identifying the phase (water droplet or ice particle) of clouds.

The CART Raman lidar uses a Nd:YAG laser operated with third-harmonic generation to produce a 355-nm (near-uv) output beam. Dichroic beamsplitters located after the receiving telescope separate the backscattered photons into three channels: the water-vapor Raman return at 408 nm, the nitrogen Raman return at 387 nm, and the combined Rayleigh/aerosol return at 355 nm. Dual-field-of-view design and high-transmission, narrowband interference filters provide excellent daytime capabilities without sacrificing nighttime performance. The entire system is computer-automated using a LabVIEW-based program; after the operator responds to a few dialog boxes during system start-up, no further operator attention is required.

The system is housed in a seatainer, a metal shipping container that measures approximately 8′x8′x20′. Optical access is provided by a weather-tight window in the roof of the seatainer; the window is covered by a motorized hatch during bad weather. A great deal of attention has been paid to the climate-control system to ensure reliable operation in the non-laboratory environment of the CART site.

The initial design of the system employed photon counting for the long-range (narrow field of view) channels, and analog-to-digital conversion for the short-range (wide field of view) channels. Early experimentation using the photon-counting electronics with the short-range channels demonstrated superior performance over the analog-to-digital converters, and we are converting to an all-photon-counting system.

Because the short-range photon-counting system was not yet fully operational at the time this paper was written, the profiles shown below were recorded using only the long-range channels; improved short-range performance (the lowest few hundred meters in particular) will follow soon. The finest vertical resolution is 39 m, determined by the minimum bin time of the photon-counting electronics. The nominal temporal resolution is one minute, although measurement periods as short as 10-30 seconds are possible. Because the system literally counts photons in equal-sized spatial and temporal bins, information is always recorded with 39-m vertical and (nominal) one-minute temporal resolution. However, *during post-acquisition signal processing*, additional averaging can be performed to trade off spatial and/or temporal resolution for improved sensitivity. In particular, this makes it possible to take advantage of the slower (in time and in space) variation of water vapor at higher altitudes to obtain higher sensitivity by post-acquisition averaging, while still having the high-resolution measurements at lower altitude.

The first measurements performed with this system at the SGP CART site were recorded during the ARESE campaign. Figures 1 and 2 show a nighttime water-vapor profile recorded at 9:30 pm (local time) on October 15, 1995. The lidar profile represents a ten-minute average started when the radiosonde was launched. Altitude-dependent averaging was applied, producing 78-m resolution from 0-1 km, 39-m resolution from 1-4 km, 78-m resolution from 4-6 km, 156-m resolution from 6-10 km, and 312-m resolution from 10-12 km. The error bars shown at these intervals were calculated using Poisson statistics for the observed photon counts. Figure 1 is plotted using a linear scale for the abscissa to demonstrate the excellent agreement with the radiosonde measurement, and Figure 2 is plotted using a logarithmic scale for the abscissa to demonstrate the performance of the system in the upper troposphere.

Figure 3 shows a daytime water-vapor profile recorded at 12:30 pm (local time) the following day, October 16, 1995. Altitude-dependent averaging was again applied, producing 78-m resolution from 0-0.7 km, 39-m resolution from 0.7-1.5 km, 78-m resolution from 1.5-3 km, 156-m resolution from 3-4 km, and 312-m resolution from 4-6 km. The relatively large error bars near zero altitude will be significantly reduced when the low-channel photon counters become operational. The divergence between the lidar and radiosonde profiles from 3-6 km may be due to sampling of different atmospheric regions as the radiosonde blows downwind from the directly zenith-pointing profile measured by the lidar, or it may be due to difficulties in extracting the small Raman signal

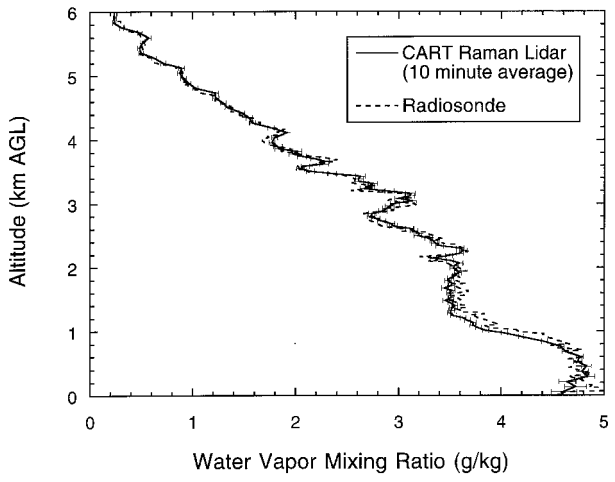

Figure 1. Nighttime profiles of water vapor recorded at the SGP CART site at 9:30 pm (local time) on October 15, 1995.

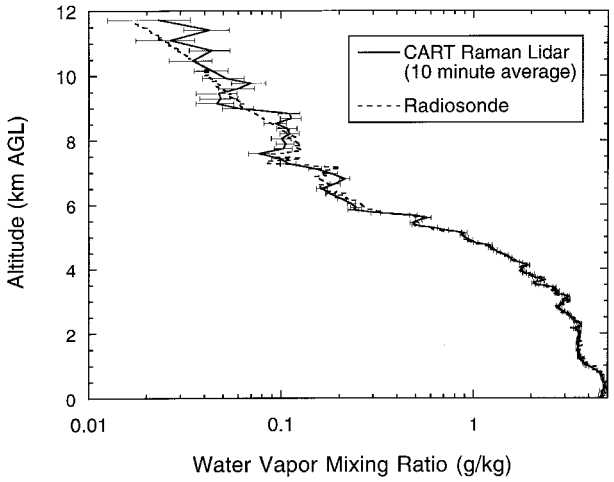

Figure 2. Nighttime profiles of water vapor recorded at the SGP CART site at 9:30 pm (local time) on October 15, 1995. This figure presents the same measurement shown in Figure 1, but extended to longer range and using a logarithmic abscissa to emphasize the performance of the system in the upper troposphere.

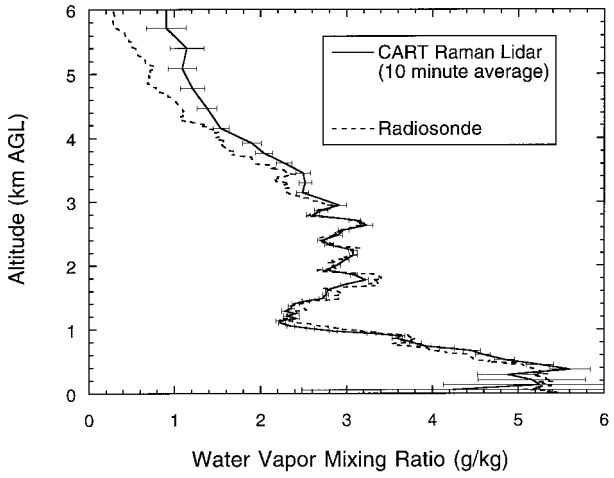

Figure 3. Daytime profiles of water vapor recorded at the SGP CART site at 12:30 pm (local time) on October 16, 1995.

from the large solar background; this question will be investigated closely using future measurements.

Although the system was operated during ARESE, damage problems in the Nd:YAG laser optics limited the operation

me and required sending the laser back to the manufacturer after the campaign. As of the writing of this paper, the laser has been repaired and the system is again operational. Our goal is to train the CART-site personnel in the operation of the system before the April 1996 intensive observation period (IOP) so that they can operate the system during and after the IOP. We anticipate detailed calibration and characterization of the CART Raman lidar through a series of IOPs that emphasize water-vapor measurements, using both native CART instruments, and other systems brought in specifically to provide additional capabilities to characterize atmospheric water vapor.